10.24425/acs.2026.158420

Archives of Control Sciences
Volume 36(LXXII), 2026
No. 1, *pages 23–54*

A new 4-D hyperchaotic Lü system with a curve equilibrium, its bifurcation analysis, multistability, circuit simulation and synchronization via integral sliding mode control

Sundarapandian VAIDYANATHAN, Fareh HANNACHI, Irene M. MOROZ, Mohamad Afendee MOHAMED, Aceng SAMBAS and R. BULLIBABU

In this research work, we first obtain a new 3-D chaotic Lü system by modifying the dynamics of the classical Lü chaotic system (2002). Next, by introducing a state feedback to the new 3-D modified Lü chaotic system, we obtain a new 4-D hyperchaotic Lü system with a curve equilibrium. We carry out a detailed bifurcation analysis of the new 4-D hyperchaotic system with a curve equilibrium and describe the bifurcation transition diagrams and Lyapunov exponents diagrams. We also derive new multistability results of the new 4-D hyperchaotic Lü system with a curve equilibrium. For engineering applications, we provide an electronic circuit simulation of the proposed hyperchaotic Lü system using MultiSim 14.0. As a control application, we derive new results for the complete synchronization for a pair of new hyperchaotic Lü systems taken as the master and slave systems. We have used integral sliding mode control for the derivation of

S. Vaidyanathan (corresponding author, e-mail: sundar@veltech.edu.in) is with Centre for Control Systems, Vel Tech University, 400 Feet Outer Ring Road, Avadi, Chennai-600062 Tamil Nadu, India and Faculty of Information and Computing, Universiti Sultan Zainal Abidin Terengganu, Malaysia.

F. Hannachi (e-mail: fareh.hannachi@univ-tebessa.dz) is with Department of Management Sciences, Echahid Cheikh Larbi Tebessi University, Route de Constantine, 12022, Tebessa, Algeria.

I.M. Moroz (e-mail: Irene.Moroz@maths.ox.ac.uk) is with Mathematical Institute, University of Oxford, Andrew Wiles Building, ROQ, Oxford Ox2 6GG, UK.

M.A. Mohamed (e-mail: mafendee@unisza.edu.my) is with Faculty of Information and Computing, Universiti Sultan Zainal Abidin, Terengganu, Malaysia.

A. Sambas (e-mails: acengsambas@unisza.edu.my, acengs@umtas.ac.id) is with Faculty of Informatics and Computing, Universiti Sultan Zainal Abidin, Gong Badak, 21300, Terengganu, Malaysia and Department of Mechanical Engineering, Universitas Muhammadiyah Tasikmalaya, Jawa Barat 46196, Indonesia.

R. Bullibabu (e-mail: drbullibabur@gmail.com) is with Department of Artificial Intelligence, Machine Learning and Data Science, KITS Akshar Institute of Technology, NH-16, Yanamadala, Guntur-522019, Andhra Pradesh, India.

Received 11.5.2025.

the synchronizing control law for the complete synchronization design for the new hyperchaotic Lü system. MATLAB simulations are provided to illustrate the main results of this research work.

Key words: chaos, chaotic systems, curve equilibrium, bifurcation, multistability, circuit design, synchronization, sliding mode control

1. Introduction

Nonlinear dynamical systems with at least two positive Lyapunov exponents are referred to as hyperchaotic systems in the control literature [1]. Chaotic dynamical systems have several applications like quantum systems [2, 3], memristors [4, 5], encryption [6, 7], fuzzy systems [8, 9], neural networks [10, 11], robotics [12], etc.

In the chaos-related literature, significant interest has been made in the construction of hyperchaotic systems with infinitely many equilibrium points [13]. Chen and Yang [14] presented a new hyperchaotic Lorenz system with a curve of equilibrium points. Vaidyanathan *et al.* [15] described modeling and FPGA implementation of a 5D hyperchaotic weather fluctuation model with a line of equilibrium points. In addition, significant attention has been made by scientists in designing chaotic or hyperchaotic systems with curves of equilibrium points such as line equilibrium [16, 17], circle equilibrium [18], capsule-shaped equilibrium [19], parabolic equilibrium [20], etc.

In this research work, we first introduce a new 3-D chaotic Lü system by modifying the dynamics of a classical Lü chaotic system ([21], 2002). Next, by introducing a state feedback to the new 3-D modified Lü chaotic system, we derive a new 4-D hyperchaotic Lü system with a curve equilibrium.

We present a detailed stability analysis and bifurcation analysis of the new 4-D hyperchaotic Lü system with curve equilibrium and describe bifurcation transition diagrams and Lyapunov exponents diagrams. Bifurcation analysis of hyperchaotic systems helps in understanding the various qualitative properties of dynamical systems [22, 23]. Multistability of chaotic or hyperchaotic systems refers to the coexistence of chaotic or hyperchaotic attractors for the same values of the system parameters, but for varying initial states of the systems [24, 25]. We also derive new multistability results of the new 4-D hyperchaotic Lü system with a curve equilibrium.

For engineering applications, we provide an electronic circuit simulation of the proposed hyperchaotic Lü system using MultiSim. Circuit designs of chaotic and hyperchaotic systems are very useful for real-world applications of the hyperchaotic systems [26–28].

Sliding mode control (SMC) is a popular nonlinear control technique featuring excellent properties of accuracy, robustness, and easy tuning and implementation [29,30]. The goal of designing a sliding mode control (SMC) is to drive the system states onto a particular surface in the state space, named sliding surface. Once the sliding surface is reached, SMC keeps the states on the close neighbourhood of the sliding surface. Sliding mode control has many applications in control of chaotic systems [31].

In this research work, we derive new results for the synchronization of a pair of new hyperchaotic Lü systems taken as the master and slave systems. We use integral sliding mode control for the derivation of the synchronizing control law for the complete synchronization design for the new hyperchaotic Lü system. Synchronization of hyperchaotic systems has important applications in engineering applications such as secure communications [32, 33]. MATLAB simulations are provided to illustrate the main results of this research work.

2. A new 4-D hyperchaotic Lü system with a curve equilibrium

In 2002, Lü and Chen [21] found a 3-D chaotic system with a two-scroll chaotic attractor and having the following dynamics:

$$\begin{cases} \dot{x} = a(y - x), \\ \dot{y} = cy - xz, \\ \dot{z} = xy - bz. \end{cases} \tag{1}$$

Here, $X = (x, y, z)$ is the 3-D state and a, b, c are positive constants for the Lü system (1).

Lü and Chen showed that the 3-D system (1) is chaotic and exhibits a two-scroll attractor for the values of the constants:

$$a = 36, \quad b = 3, \quad c = 20. \tag{2}$$

For $X(0) = (0.4, 0.2, 0.4)$ and the constant values as in (2), the Lyapunov exponents of the 3-D Lü system (1) were computed for $T = 1E4$ seconds as $L_1 = 1.3435$, $L_2 = 0$ and $L_3 = -20.2807$.

This shows that the 3-D system derived by Lü and Chen [1] is a chaotic and dissipative system. In this research work, we modify the Lü system (1) by subtracting a linear term in the second differential equation as follows:

$$\begin{cases} \dot{x} = a(y - x), \\ \dot{y} = cy - px - xz, \\ \dot{z} = xy - bz. \end{cases} \tag{3}$$

Also, we take the values of parameters as follows:

$$a = 53, \quad b = 12, \quad c = 32, \quad p = 2. \tag{4}$$

For $X(0) = (0.4, 0.2, 0.4)$ and the constant values as in (4), the Lyapunov exponents of the new 3-D system (3) were computed for $T = 1E4$ seconds as $L_1 = 2.0126$, $L_2 = 0$ and $L_3 = -35.0126$. This shows that the new 3-D system (3) is chaotic and dissipative.

Since the maximal Lyapunov exponent (MLE) of the new 3-D system (3) is higher than the MLE of the Lü system (1), the new chaotic system (3) has more complexity than the Lü system (1).

Since the new chaotic system (3) remains invariant under the coordinates map $(x, y, z) \mapsto (-x, -y, z)$, we deduce that the new 3-D system (3) also has rotation symmetry about the z-axis.

The equilibrium points of the new chaotic system (3) are obtained by solving the equations:

$$a(y - x) = 0, \tag{5a}$$

$$cy - px - xz = 0, \tag{5b}$$

$$xy - bz = 0. \tag{5c}$$

From (5a), we get $y = x$. Substituting this into (5c), we get

$$z = \frac{x^2}{b}. \tag{6}$$

Also, (5b) can be simplified as follows:

$$(c - p)x - \frac{x^3}{b} = 0 \ \text{ or } \ x\left[(c - p) - \frac{x^2}{b}\right] = 0. \tag{7}$$

Thus, there are three roots for x, *viz.*

$$x = 0 \ \text{ or } \ x = \pm\sqrt{b(c - p)}. \tag{8}$$

Thus, the new chaotic system (3) has three real equilibrium points (when $c > p$):

$$P_1 = \begin{bmatrix} 0 \\ 0 \\ 0 \end{bmatrix}, \quad P_2 = \begin{bmatrix} \sqrt{b(c-p)} \\ \sqrt{b(c-p)} \\ c - p \end{bmatrix}, \quad P_3 = \begin{bmatrix} -\sqrt{b(c-p)} \\ -\sqrt{b(c-p)} \\ c - p \end{bmatrix}. \tag{9}$$

For the chaotic case $(a, b, c, p) = (53, 12, 32, 2)$, the equilibria of the new chaotic system (3) are obtained as follows:

$$P_1 = \begin{bmatrix} 0 \\ 0 \\ 0 \end{bmatrix}, \quad P_2 = \begin{bmatrix} 18.9737 \\ 18.9737 \\ 30 \end{bmatrix}, \quad P_3 = \begin{bmatrix} -18.9737 \\ -18.9737 \\ 30 \end{bmatrix}. \tag{10}$$

The eigenvalues of the Jacobian matrix of the system (3) at P_1 are obtained as -12, -51.7341 and 30.7341, which shows that P_1 is an unstable saddle point equilibrium of the system (3). The eigenvalues of the Jacobian matrix of the system (3) at P_2 are found as -40.8707 and $3.9353 \pm 30.3017i$, which shows that P_2 is an unstable, saddle-focus point equilibrium of the system (3). The eigenvalues of the Jacobian matrix of the system (3) at P_3 are obtained as -40.8707 and $3.9353 \pm 30.3017i$, which shows that P_3 is also an unstable, saddle-focus point equilibrium of the system (3).

MATLAB plots of the new chaotic system (3) for the initial state $(0.4, 0.2, 0.4)$ and the parameter set $(a, b, c, p) = (53, 12, 32, 2)$ are depicted in Figures 1 and 2.

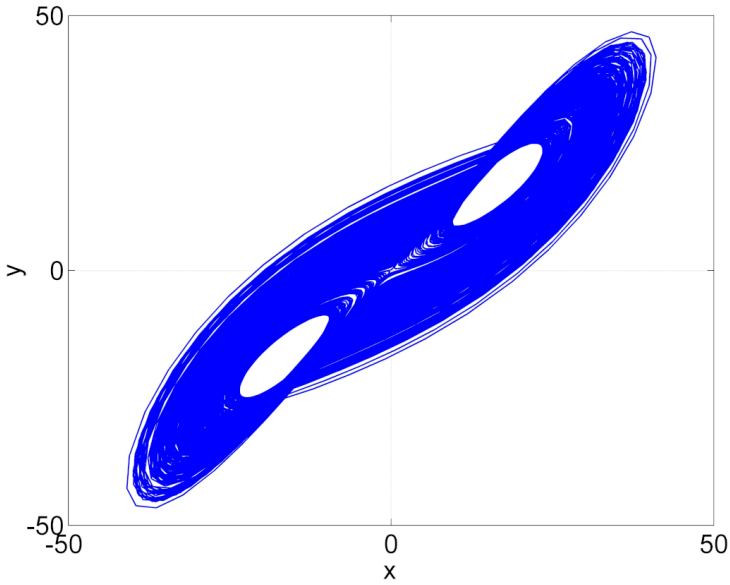

Figure 1: (x, y) plot of the new chaotic system (3) for $X(0) = (0.4, 0.2, 0.4)$ and $(a, b, c, p) = (53, 12, 32, 2)$.

The new chaotic system (3) exhibits a two-scroll chaotic attractor as it is a modified version of the Lü chaotic system (1).

In this research work, we design a new 4-D hyperchaotic system with a curve equilibrium by introducing a feedback control into the 3-D chaotic system (3).

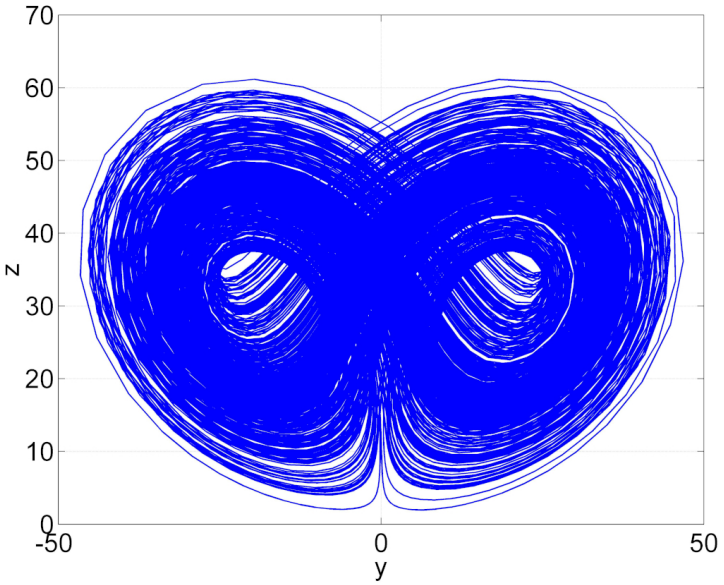

Figure 2: (y, z) plot of the new chaotic system (3) for $X(0) = (0.4, 0.2, 0.4)$ and $(a, b, c, p) = (53, 12, 32, 2)$

By introducing a feedback control into the 3-D chaotic dynamics (3), we propose a new 4-D system described as follows:

$$\begin{cases} \dot{x} = a(y - x), \\ \dot{y} = cy - px - xz + w, \\ \dot{z} = xy - bz, \\ \dot{w} = (c - p)x - \dfrac{x^3}{b} + w. \end{cases} \tag{11}$$

In the system (11), a, b, c, p are positive bifurcation parameters. We denote $X = (x, y, z, w)$ to represent the 4-D state of the new 4-D system (11).

In this work, we shall show that the new 4-D system (11) is *hyperchaotic* for the constant values chosen as

$$a = 74, \quad b = 18, \quad c = 40, \quad p = 3. \tag{12}$$

For $X(0) = (0.4, 0.2, 0.4, 0.2)$ and the parameter values as in (12), the Lyapunov exponents of the new 4-D system (11) were computed for $T = 1E4$ seconds as follows:

$$L_1 = 2.2537, \quad L_2 = 0.2140, \quad L_3 = 0, \quad L_4 = -53.4656. \tag{13}$$

From (13), we conclude that the 4-D system (11) is a hyperchaotic system with the maximal Lyapunov exponent (MLE) obtained by $L_{\max} = 2.2537$, which is greater than the MLE ($L_{\max} = 2.0126$) of the 3-D chaotic system (3) and the MLE ($L_{\max} = 1.3435$) of the 3-D Lü chaotic system (1).

Thus, the 4-D hyperchaotic system (11) with two positive Lyapunov exponents exhibits more complexity than the 3-D chaotic systems given by the dynamics (1) and (3).

Also, the Kaplan dimension of the 4-D hyperchaotic system (11) is found as follows:

$$D_K = 3 + \frac{1}{|L_4|}(L_1 + L_2 + L_3) = 3.0462. \tag{14}$$

The divergence of the flow of the new 4-D hyperchaotic system (11) is calculated as follows:

$$\nabla \cdot (\dot{x}, \dot{y}, \dot{z}, \dot{w}) = -a + c - b + 1 < 0 \tag{15}$$

for contracting flows. For the hyperchaotic case (12), the divergence of the flow of (11) is found as

$$\nabla \cdot (\dot{x}, \dot{y}, \dot{z}, \dot{w}) = -74 + 40 - 18 + 1 = -51 < 0, \tag{16}$$

which is strongly contracting.

In contrast, for the Lü system (1), the divergence of the flow for the chaotic case $(a, b, c) = (36, 3, 20)$ is obtained as

$$\nabla \cdot (\dot{x}, \dot{y}, \dot{z}, \dot{w}) = -a + c - b = -36 + 20 - 3 = -19, \tag{17}$$

which is contracting.

Also, for the new chaotic system (3), the divergence of the flow for the chaotic case $(a, b, c, p) = (53, 12, 32, 2)$ is obtained as

$$\nabla \cdot (\dot{x}, \dot{y}, \dot{z}, \dot{w}) = -a + c - b = -53 + 32 - 12 = -33, \tag{18}$$

which is contracting.

Next, we calculate the equilibrium points of the 4-D hyperchaotic system (11) by solving the following equations:

$$a(y - x) = 0, \tag{19a}$$

$$cy - px - xz + w = 0, \tag{19b}$$

$$xy - bz = 0, \tag{19c}$$

$$(c - p)x - \frac{x^3}{b} + w = 0. \tag{19d}$$

From (19a), we get

$$y = x. \tag{20}$$

Substituting $y = x$ from (20) in Eq. (19c), we get

$$z = \frac{x^2}{b}. \tag{21}$$

Substituting from (20) and (21) into (19b), we get

$$w = (p - c)x + \frac{x^3}{b}. \tag{22}$$

which satisfies Eq. (19d).

Thus, we conclude that the new 4-D hyperchaotic system (11) has a curve of equilibrium points given by

$$S = \left\{ X \in \mathbb{R}^4 : y = x, z = \frac{x^2}{b}, w = (p - c)x + \frac{x^3}{b}, \text{ where } x \in \mathbb{R} \right\}. \tag{23}$$

Hence, we deduce that the new 4-D hyperchaotic system (11) has hidden attractors.

MATLAB simulations are provided in Figures 3 to 6 for the 4-D hyperchaotic system (11) when $X(0) = (0.4, 0.2, 0.4, 0.2)$ and $(a, b, c, p) = (74, 18, 40, 3)$.

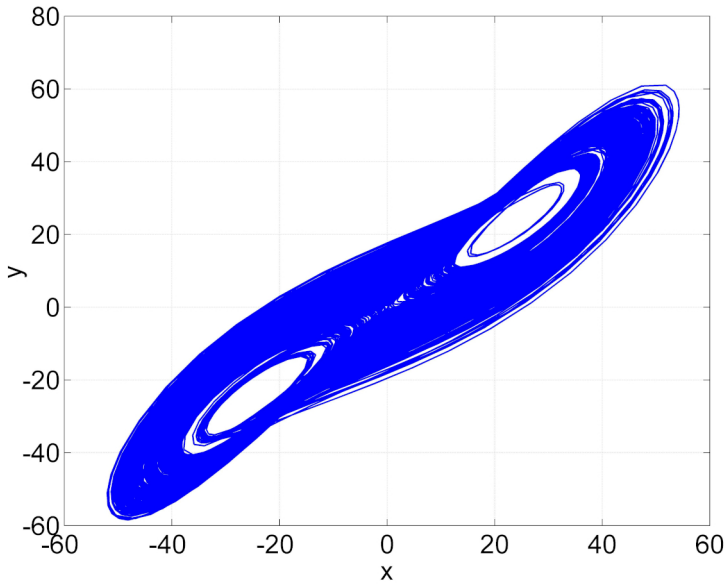

Figure 3: (x, y) plot of the new hyperchaotic system (11) for $X(0) = (0.4, 0.2, 0.4, 0.2)$ and $(a, b, c, p) = (74, 18, 40, 3)$

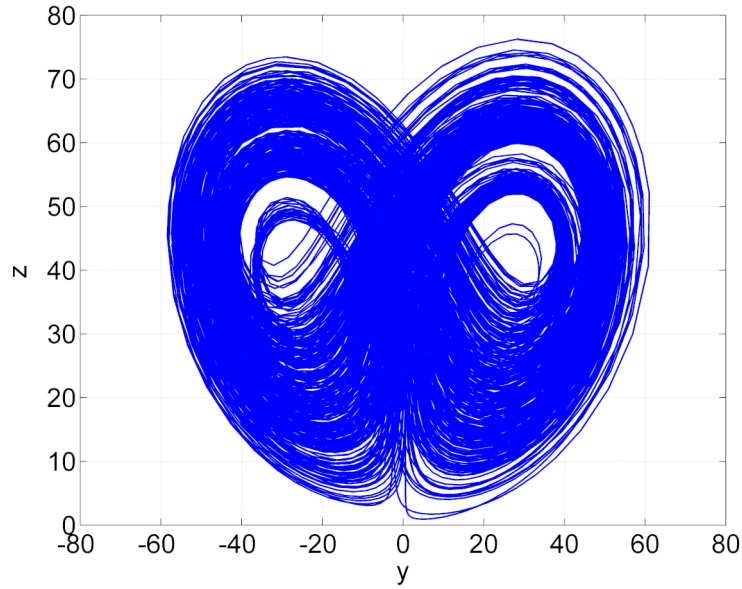

Figure 4: (y, z) plot of the new hyperchaotic system (11) for $X(0) = (0.4, 0.2, 0.4, 0.2)$ and $(a, b, c, p) = (74, 18, 40, 3)$

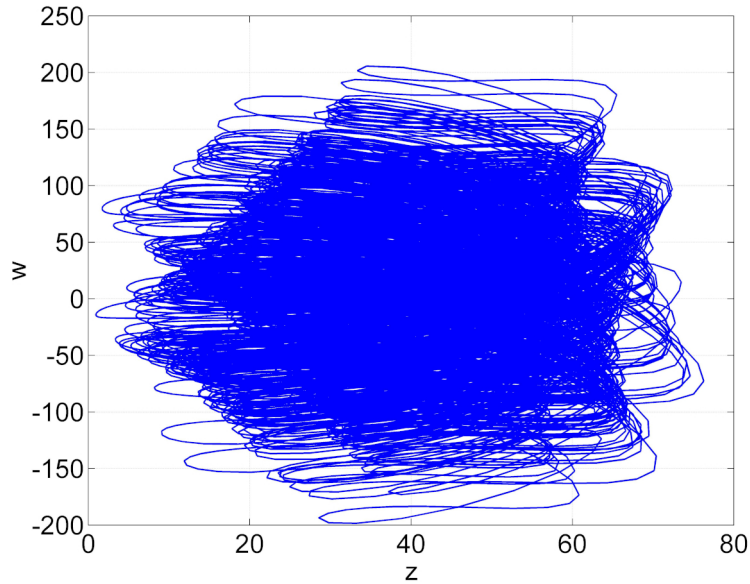

Figure 5: (z, w) plot of the new hyperchaotic system (11) for $X(0) = (0.4, 0.2, 0.4, 0.2)$ and $(a, b, c, p) = (74, 18, 40, 3)$

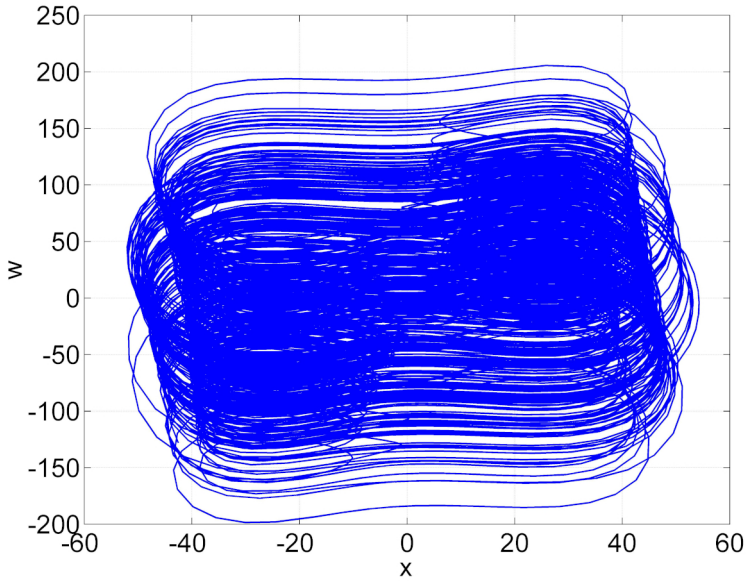

Figure 6: (x, w) plot of the new hyperchaotic system (11) for $X(0) = (0.4, 0.2, 0.4, 0.2)$ and $(a, b, c, p) = (74, 18, 40, 3)$

3. Bifurcation transition diagrams for the new hyperchaotic system

Figure 7 shows the bifurcation transition diagrams as c varies for the chaotic system (3) when (a) $p = 0$ [Lü system (1)] and (b) $p = 2$ for the parameter values $(a, b, p) = (36, 3, 2)$. Trajectories diverge to infinity when $c \approx 35.31$. Llibre et al [34] investigated the Poincaré sphere at infinity for a closely related 3D system. The two bifurcation transition plots are very similar for $c > 19.27$, but differ in the location and extent of the periodic windows for $c < 19.27$. The upper plot loses stability to a steady state when $c \approx 12.56$, while that occurs for $c \approx 13.47$ when p is included.

Figure 8 shows the bifurcation transition diagram as c varies for the 4-D system (11) with the parameter choice $(a, b, p) = (36, 3, 2)$. There are again regions of chaotic behavior, separated by periodic windows, with a loss of stability to steady states when $c \approx 16.61$.

Finally, Figure 9 shows the corresponding bifurcation transition diagram for c for the 4D system (11) with the chosen set of parameter values $(a, b, p) = (74, 18, 3)$. The number of periodic windows has diminished in Figure 9, with a loss of stability to steady states when $c \approx 28.82$.

We investigated a 4D nonlinear extension to the Lü system [21] in a manner in which the new fourth variable is defined by a cubic curve of equilibrium states in

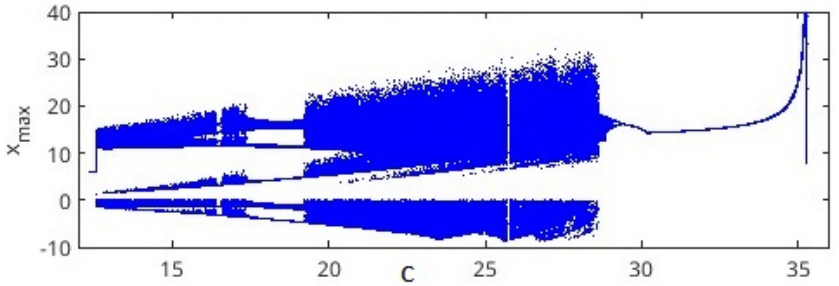

(a)

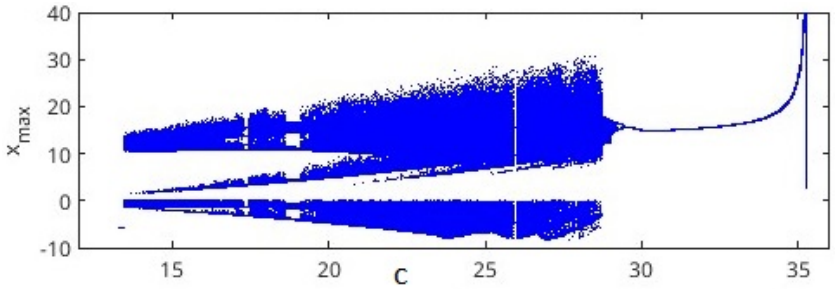

(b)

Figure 7: The bifurcation transition plot of the state $x_{\max}$ as c varies between (a) $12.58 \approx c \approx 35.31$ for the Lü system (1) (b) $13.49 \approx c \approx 35.31$ for the modified Lü system (3) with $(a, b, p) = (36, 3, 2)$. The solution diverges for $c \approx 23.57$, when $x_{\max} \approx 1164.972$

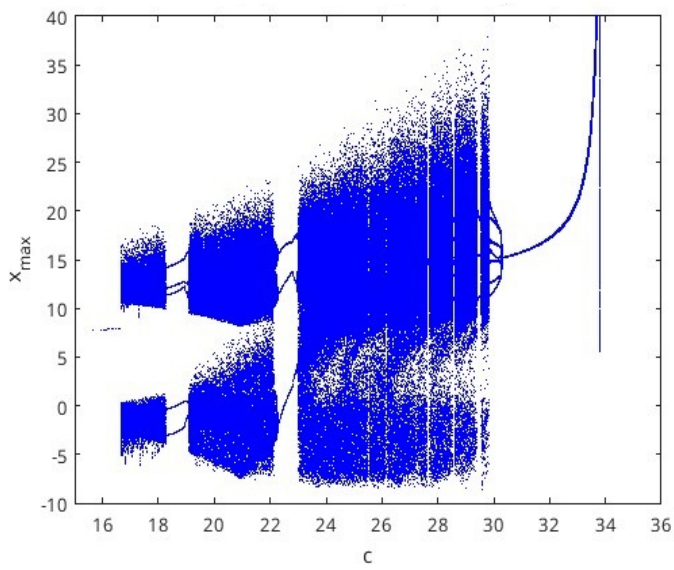

Figure 8: The bifurcation transition plot of the state $x_{\max}$ as c varies between $15.94 < c < 33.79$ for the 4D system (11) with the parameter values $(a, b, p) = (36, 3, 2)$

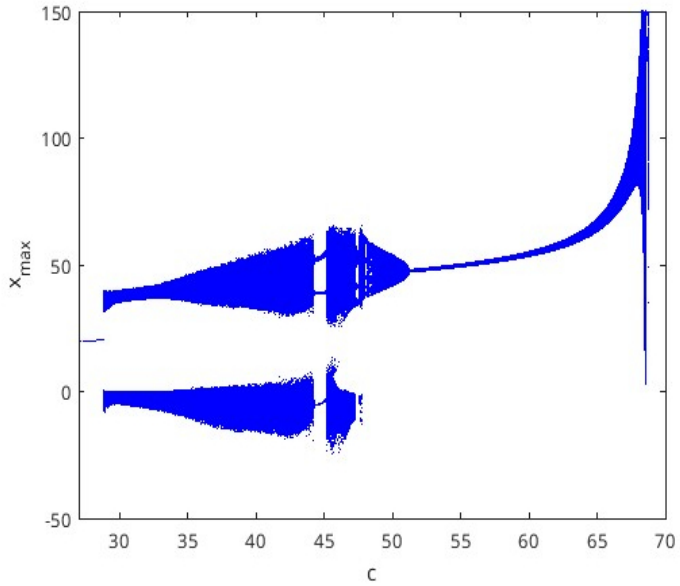

Figure 9: The bifurcation transition plot of the state $x_{\max}$ as c varies between $27.31 \approx c \approx 68.53$ for the 4D system (11) with the parameter values $(a, b, p) = (74, 18, 3)$

terms of the x-variable. The other two variables have equilibria, defined explicitly in terms of x.

Bifurcation transition plots as the parameter c varies show large regions of chaotic dynamics and periodic windows. We compared these plots with plots for the original Lü system (1) and its extension (3) which include an additional linear term $-px$ in the equation for the evolution of y. The bifurcation transition plots are very similar for $c > 19.27$, but differ in the extent of periodic windows for smaller values of c. All four bifurcation transition plots show the divergence of the variable $x_{\max}$ for larger values of c.

4. Dynamic analysis of the new hyperchaotic system with a curve equilibrium

In this section, we have investigated the dynamics of the 4-D system (11) under different parameters by means of the bifurcation diagram with the Lyapunov exponents spectrum. In the hyperchaotic case, the parameter values are fixed as $(a, b, c, p) = (74, 18, 40, 3)$.

Figures 10, 11, 12 and 13 show the bifurcation plots and Lyapunov exponents spectrum of the 4-D system (11) with respect to the parameters a, b, c, p respectively.

Explicitly, we will show that when $a \in [70, 80]$, $b \in [15, 25]$, $c \in [35, 40]$ or $p \in [0, 10]$, the behaviors of the 4-D system (11) are either hyperchaotic or chaotic.

4.1. Varying the parameter a

Figure 10 shows the Lyapunov exponents spectrum and the bifurcation diagram of the new 4-D system (11) with respect to parameter a, when a

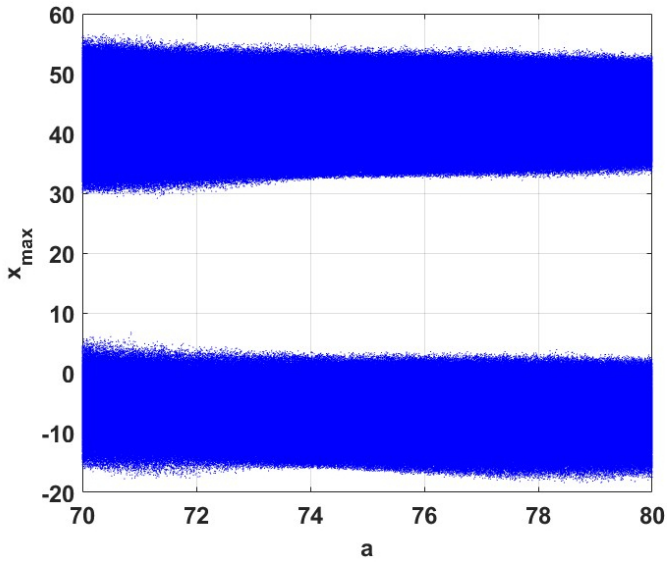

(a)

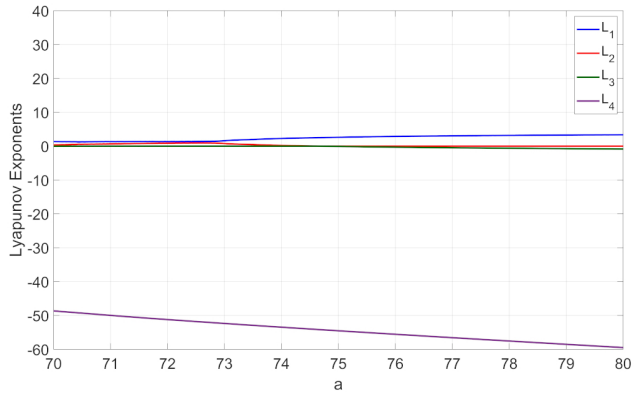

(b)

Figure 10: (a) Bifurcation diagram and (b) LE spectrum of the 4-D dynamics (11) for $a \in [70, 80]$, $b = 18$, $c = 40$ and $p = 3$

varies in the range $[70, 80]$. We fix the values of the parameters b, c and p as $(b, c, p) = (18, 40, 3)$.

We can identify the dynamic behavior of the 4-D system (11) when the parameter a varies in the range $[70, 80]$.

In Figure 10, it can be seen that the 4-D system (11) exhibits hyperchaotic behavior when $a \in [70, 74.70]$, where $L_1 > 0$, $L_2 > 0$, $L_3 = 0$ and $L_4 < 0$.

It can also be noted that system (8) exhibits chaotic behavior when $a \in [74.70, 80]$, where $L_1 > 0$, $L_2 = 0$, $L_3 < 0$ and $L_4 < 0$. The behaviors and Lyapunov exponents of the new 4D system (11) for different values of the parameter a are summarized in Table 1.

Table 1: Summary Table for behaviors and Lyapunov exponents of the new 4D system (11) for different values of parameter a, where $(b, c, p) = (18, 40, 3)$

Behavior	Parameter a	LEs			
		L_1	L_2	L_3	L_4
Chaotic	75	2.612	0	−0.08327	−54.53
	75.80	2.819	0	−0.2647	55.35
	77.50	3.109	0	−0.5478	−57.06
	78.86	3.2620	0	−0.7248	−58.39
	70	1.3480	0.3269	0	−48.65
	70.50	1.2790	0.5459	0	−49.32
	79.30	3.30	0	−0.7759	−58.82
	80	3.3480	0	−0.8551	−59.49
Hyperchaotic	71.60	1.3480	0.7972	0	−50.74
	72	1.3510	0.8674	0	−51.22
	72.40	1.3720	0.9167	0	−51.69
	72.80	1.4360	0.9059	0	−52.14
	73.70	2.1090	0.3364	0	−53.14
	73.90	2.2130	0.2454	0	−53.36

4.2. Varying the parameter b

Figure 11 shows the Lyapunov exponents spectrum and the bifurcation diagram of the new 4-D system (11) with respect to parameter b, when b varies in the range $[15, 25]$. We fix the values the parameters a, c and p as $(a, c, p) = (74, 40, 3)$.

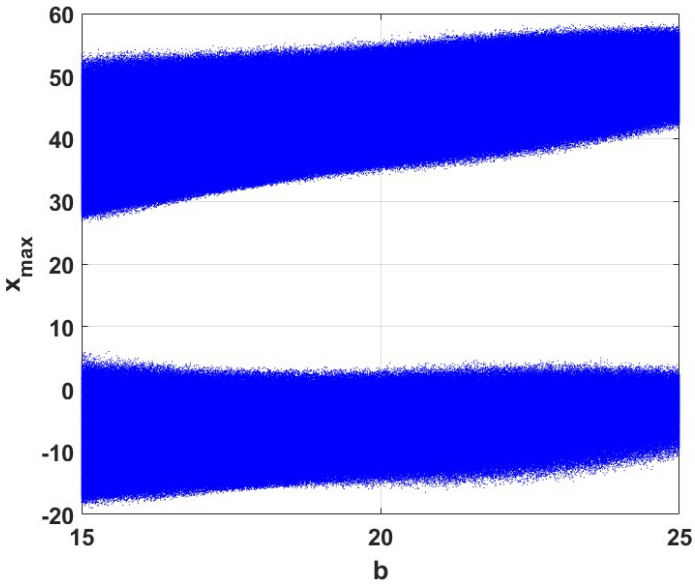

(a)

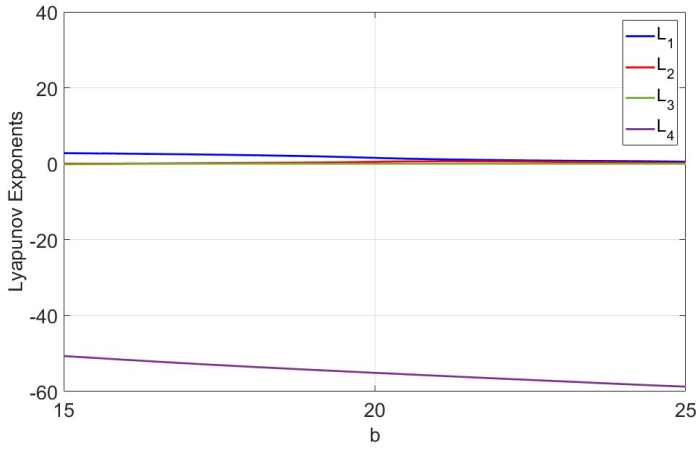

(b)

Figure 11: (a) Bifurcation diagram and (b) LE spectrum of the 4-D dynamics (11) for $b \in [15, 25]$, $a = 74$, $c = 40$ and $p = 3$

In Figure 11, it can be seen that the 4-D system (11) exhibits hyperchaotic behavior when $b \in [15, 25]$, where $L_1 > 0$, $L_2 > 0$, $L_3 = 0$ and $L_4 < 0$.

The behaviors and Lyapunov exponents of the new system (11) for different values of the parameter b are summarized in Table 2.

Table 2: Summary Table for behaviors and Lyapunov exponents of the new 4D system (11) for different values of parameter b, where $(a, c, p) = (74, 40, 3)$

Behavior	Parameter b	LEs			
		L_1	L_2	L_3	L_4
Hyperchaotic	15	2.2775	0.0192	−0.1453	−50.65
	15.28	2.750	0.01988	−0.1273	−50.92
	15.60	2.7070	0.02719	−0.0953	-51.24
	16	2.6560	0.03747	−0.04748	−51.64
	17	2.4860	0.1097	0	-52.59
	17.80	2.3070	0.1911	0	−53.30
	18.20	2.2120	0.2248	0	−53.63
	18.60	2.1070	0.2589	0	−53.96
	20	1.5860	0.4996	0	−55.88
	21	1.1860	0.6428	0	−55.83
	23	0.8022	0.5142	0	−57.31
	24	0.6927	0.3537	0	−58.04
	25	0.5223	0.1634	0	−58.68

4.3. Varying the parameter c

Figure 12 shows the Lyapunov exponents spectrum and the bifurcation diagram of the new 4-D system (11) with respect to parameter c, when c varies in the range $[35, 40]$. We fix the values the parameters a, b and p as $(a, b, p) = (74, 18, 3)$.

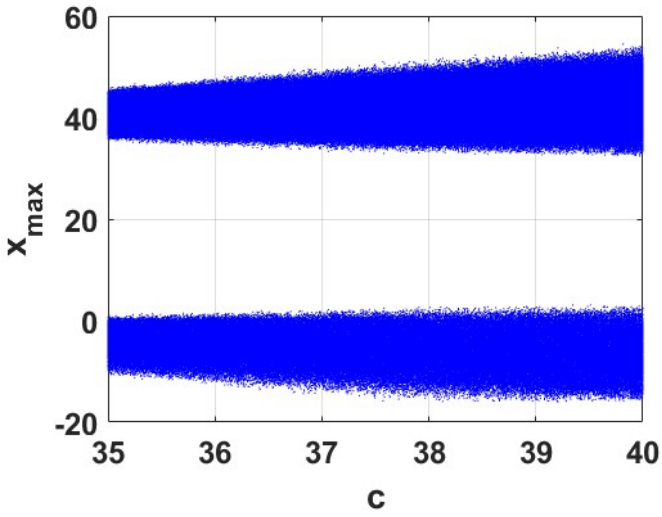

(a)

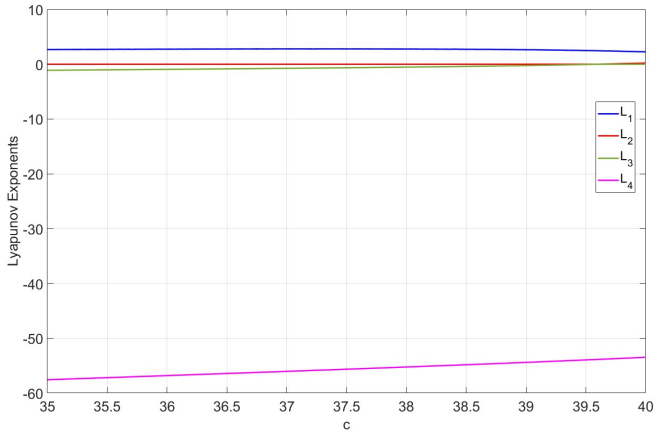

(b)

Figure 12: (a) Bifurcation diagram and (b) LE spectrum of the 4-D dynamics (11) for $c \in [35, 40]$, $a = 74$, $b = 18$ and $p = 3$

In Figure 12, it can be seen that the 4-D system (11) exhibits a chaotic behavior when $c \in [35, 39.6]$, where $L_1 > 0$, $L_2 = 0$, $L_3 < 0$ and $L_4 < 0$.

In Figure 12, it can also be seen that the 4-D system (11) exhibits a chaotic behavior when $c \in (39.6, 40]$, where $L_1 > 0$, $L_2 > 0$, $L_3 = 0$ and $L_4 < 0$.

The behaviors and Lyapunov exponents of the new system (11) for different values of parameter c are summarized in Table 3.

Table 3: Summary Table for behaviors and Lyapunov exponents of the new 4D system (11) for different values of parameter c, where $(a, b, p) = (74, 18, 3)$

Behavior	Parameter c	LEs			
		L_1	L_2	L_3	L_4
Chaotic	35	2.674	0	−1.1070	−57.56
	36	2.7450	0	−0.9389	56.80
	37	2.7980	0	−0.7489	−56.05
	38	2.7760	0	−0.5270	−55.25
	39	2.1646	0	−0.2442	−54.40
	39.50	2.4990	0	−0.04612	−53.95
Hyperchaotic	39.62	2.4490	0.01569	0	−53.84
	39.80	2.363.	0.1071	0	−53.67
	39.90	2.3140	0.1552	0	−53.57
	39.94	2.2550	0.1804	0	−53.52

4.4. Varying the parameter p

Figure 13 shows the Lyapunov exponents spectrum and the bifurcation diagram of the new 4-D system (11) with respect to parameter p, when p varies in the range $[0, 10]$. We fix the values the parameters a, b and c as $(a, b, c) = (74, 18, 40)$.

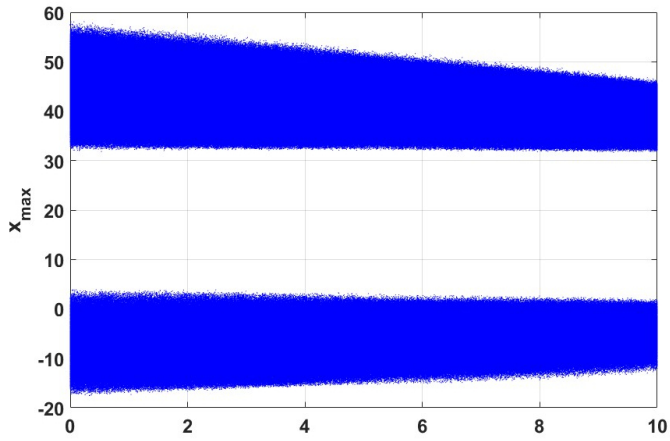

(a)

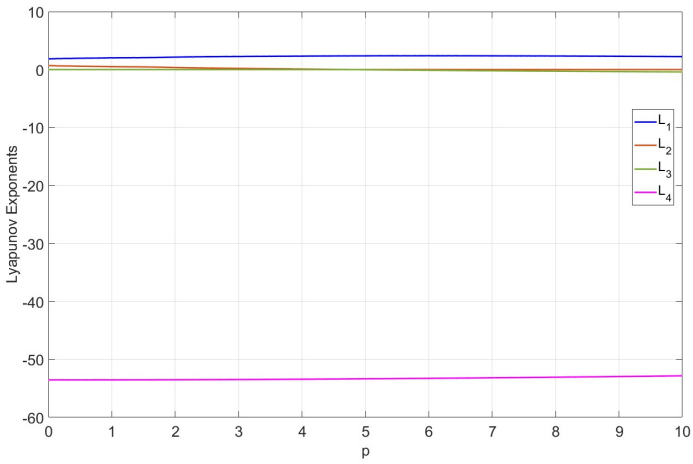

(b)

Figure 13: (a) Bifurcation diagram and (b) LE spectrum of the 4-D dynamics (11) for $p \in [0, 10]$, $a = 74$, $b = 18$ and $c = 40$

In Figure 12, it can be seen that the 4-D system (11) exhibits chaotic behavior when $c \in [35, 39.6]$, where $L_1 > 0$, $L_2 = 0$, $L_3 < 0$ and $L_4 < 0$.

In Figure 12, it can also be seen that the 4-D system (11) exhibits chaotic behavior when $c \in (39.6, 40]$, where $L_1 > 0$, $L_2 > 0$, $L_3 = 0$ and $L_4 < 0$.

The behaviors and Lyapunov exponents of the new system (11) for different values of the parameter p are summarized in Table 4.

Table 4: Summary Table for behaviors and Lyapunov exponents of the new 4D system (11) for different values of parameter p, where $(a, b, c) = (74, 18, 40)$

Behavior	Parameter p	LEs			
		L_1	L_2	L_3	L_4
Chaotic	5	2.370	0	−0.02549	−53.34
	6	2.3890	0	−0.1203	53.27
	7	2.3710	0	−0.2020	−53.17
	8	2.3450	0	−0.2754	−53.07
	9	2.2980	0	−0.3436	−52.95
	10	2.2360	0	−0.40	−52.83
Hyperchaotic	0.20	1.8920	0.6383	0	−5353
	0.50	1.9550	0.5804	0	−53.53
	1	2.031	0.5095	0	−53.54
	2	2.1480	0.3620	0	−53.51
	2.60	2.2360	0.2564	0	−53.44
	3.50	2.2920	0.1510	0	−53.44
	4	2.3220	0.08866	0	−53.41

5. Multistability and coexisting attractors for the new 4-D hyperchaotic system

A defining characteristic of integer-order chaotic systems is their capacity to display multistability, where several attractors exist simultaneously for a given set of parameters. This behavior holds considerable importance for both the study and practical use of chaotic systems. The presence of multiple attractors provides a deeper understanding of the intricate and varied dynamics of these systems, which in turn allows the creation of systems with customizable and varied dynamic characteristics.

The system (11) remains invariant under the transformation of coordinates

$$S\colon (x, y, z, w) \longrightarrow (-x, -y, z, -w). \tag{24}$$

Thus, any projection of the attractor has rotational symmetry in the z-axis.

We shall show that the 4-D system (11) exhibits coexisting hyperchaotic attractors.

Let X_1 and X_2 be two different initial conditions for the new 4-D system (11), where:

$$X_1 = (0.4, 0.2, 0.4, 0.2) \text{ (Blue color)}, \tag{25}$$

$$X_2 = (-0.4, -0.2, 0.4, -0.2) \text{ (Red color)}. \tag{26}$$

Figure 14 demonstrates the coexistence of two hyperchaotic attractors for the 4-D system (11) with different initial values where $a = 74, b = 18, c = 40, p = 3$ and initial states $X_1 = (0.4, 0.2, 0.4, 0.2)$ (blue orbit) and $X_2 = (-0.4, -0.2, 0.4, -0.2)$ (red orbit).

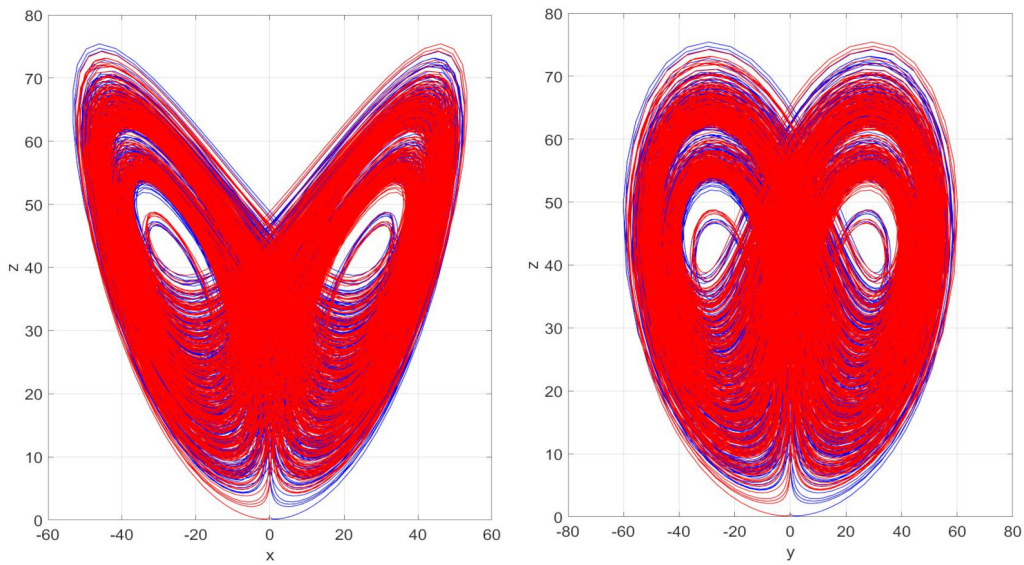

(a) (b)

Figure 14: Coexistence of two hyperchaotic attractors for the 4-D system (11) with different initial values where $a = 22, b = 2.2, c = 29, p = 1.5$: The initial states are chosen as $X_1 = (0.4, 0.2, 0.4, 0.2)$ (blue orbit) and $X_2 = (-0.4, -0.2, 0.4, -0.2)$ (red orbit)

6. Circuit simulation of the new 4D hyperchaotic system with a curve equilibrium

In this section, the new 4D chaotic system (11) is realized by the NI Multisim 14.2 platform. The electronic circuit design of the 4D hyperchaotic system (11) is shown in Figure 15 in which TLO84ACD is selected as OPAMP and the multipliers are of type AD633.

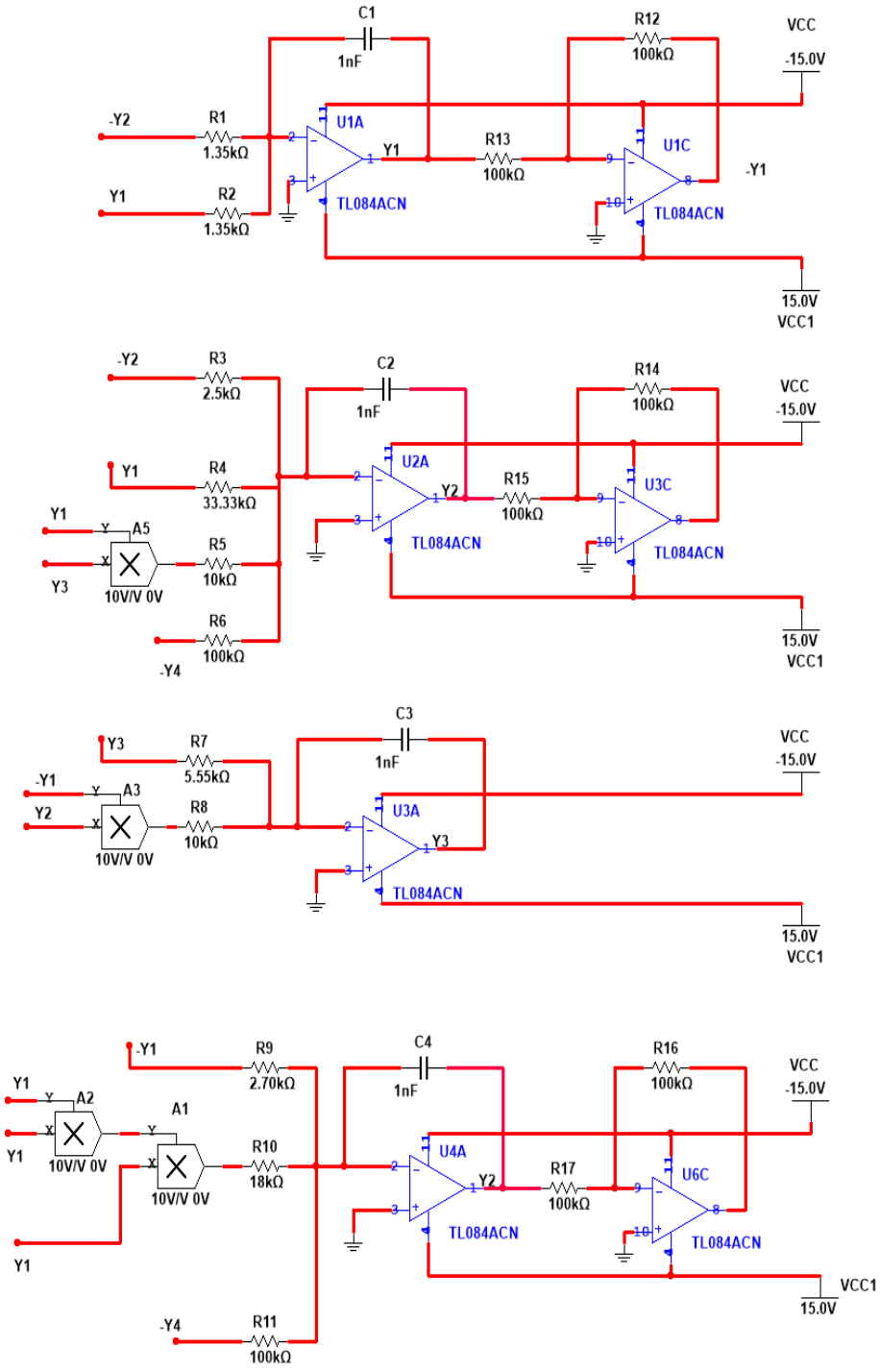

Figure 15: Circuit design of the new 4D hyperchaotic system (27) with a curve equilibrium

Using Kirchhoff's electrical circuit laws, we derive the circuit model for the rescaled 4D hyperchaotic system (8) as follows:

$$\begin{cases} \dot{y_1} = \dfrac{1}{R_1C_1}y_2 - \dfrac{1}{R_2C_1}y_1\,, \\ \dot{y_2} = \dfrac{1}{R_3C_2}y_2 - \dfrac{1}{R_4C_2}y_1 + \dfrac{1}{10R_5C_2}y_1y_3 + \dfrac{1}{R_6C_2}y_4\,, \\ \dot{y_3} = -\dfrac{1}{R_7C_3}y_3 + \dfrac{1}{10R_8C_3}y_1y_2\,, \\ \dot{y_4} = \dfrac{1}{R_9C_4}y_1 - \dfrac{1}{100R_{10}C_4}{y_1}^3 + \dfrac{1}{R_{11}C_4}y_4\,. \end{cases} \tag{27}$$

Here y_1, y_2, y_3, y_4 are the voltages across the capacitors, $C1, C2, C3, C4$, respectively.

The values of the components in the circuit are selected as follows:

$$C_1 = C_2 = C_3 = C_4 = 1 \text{ nF}, \tag{28}$$

$$R_1 = R_2 = 1.35\ \text{k}\Omega, \quad R_3 = 2.5\ \text{k}\Omega, \quad R_4 = 33.33\ \text{k}\Omega, \tag{29}$$

$$R_7 = 5.55\ \text{k}\Omega, \quad R_9 = 2.70\ \text{k}\Omega, \quad R_{10} = 18\ \text{k}\Omega, \quad R_6 = R_8 = 10\ \text{k}\Omega, \tag{30}$$

$$R_6 = R_{11} = R_{12} = R_{13} = R_{14} = R_{15} = R_{16} = R_{17} = 100\ \text{k}\Omega. \tag{31}$$

Multisim outputs of the circuit are via oscilloscope XSC1 are plotted in Figures 16 to 19. Multisim outputs of the circuit are via Tektronix oscilloscope are plotted in Figures 20 to 23.

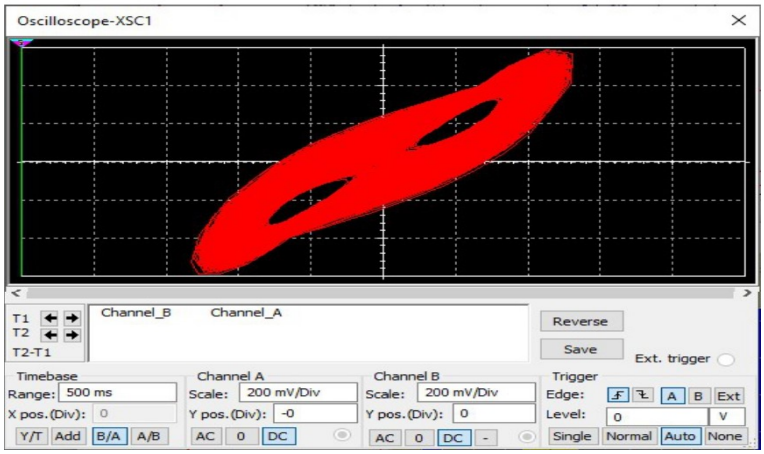

Figure 16: (x, y) plot of the new hyperchaotic system (27) via oscilloscope XSC1

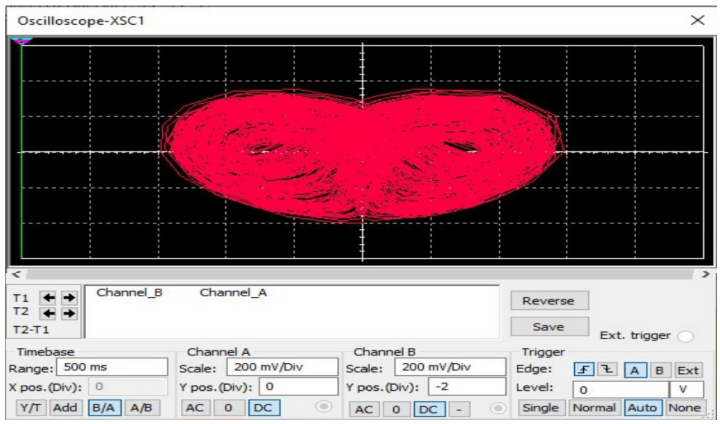

Figure 17: (y, z) plot of the new hyperchaotic system (27) via oscilloscope XSC1

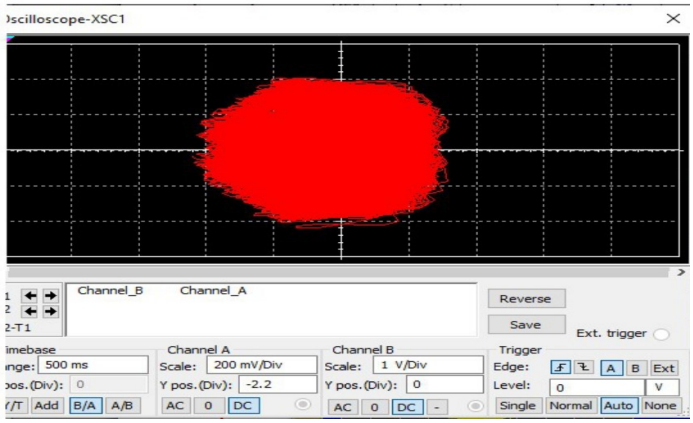

Figure 18: (z, w) plot of the new hyperchaotic system (27) via oscilloscope XSC1

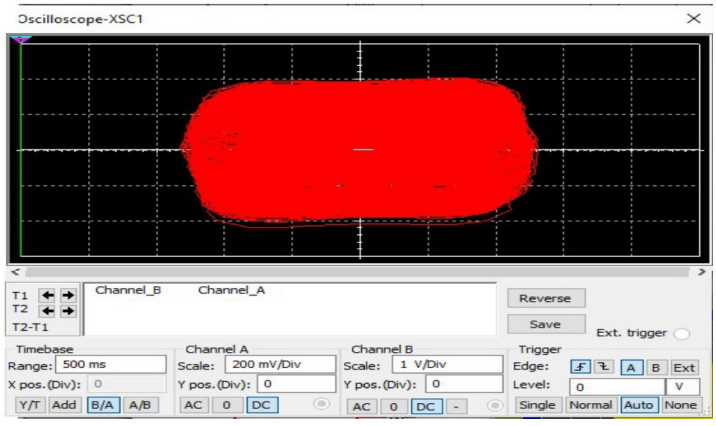

Figure 19: (x, w) plot of the new hyperchaotic system (27) via oscilloscope XSC1

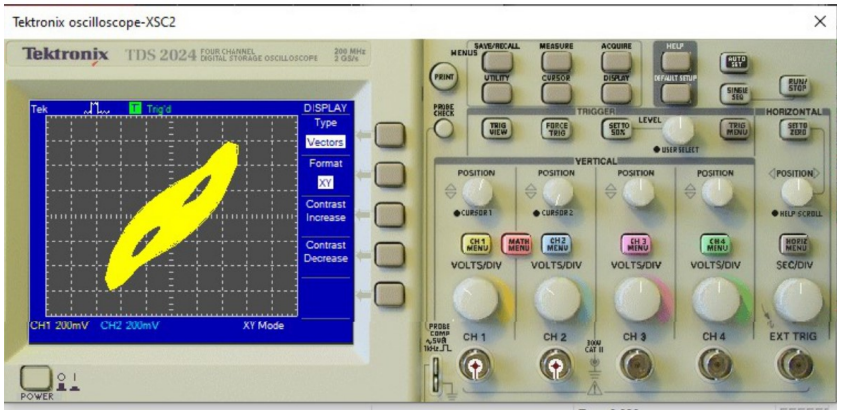

Figure 20: (x, y) plot of the new hyperchaotic system (27) via Tektronix oscilloscope

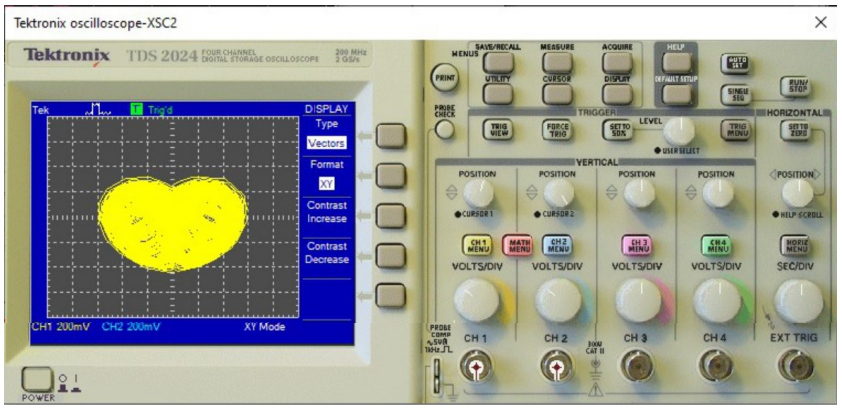

Figure 21: (y, z) plot of the new hyperchaotic system (27) via Tektronix oscilloscope

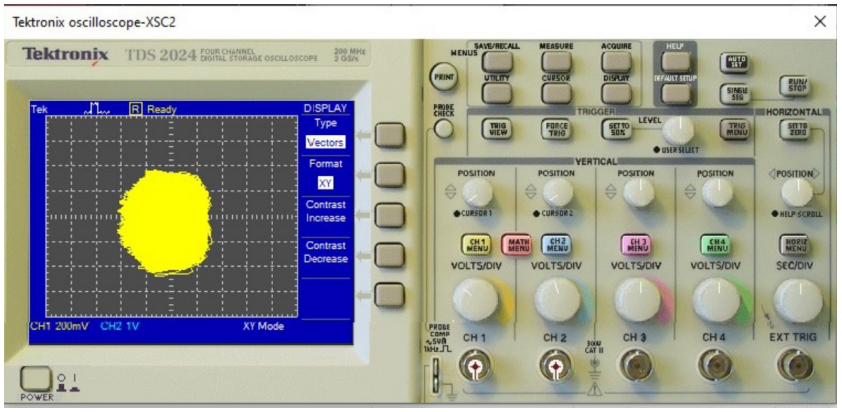

Figure 22: (z, w) plot of the new hyperchaotic system (27) via Tektronix oscilloscope

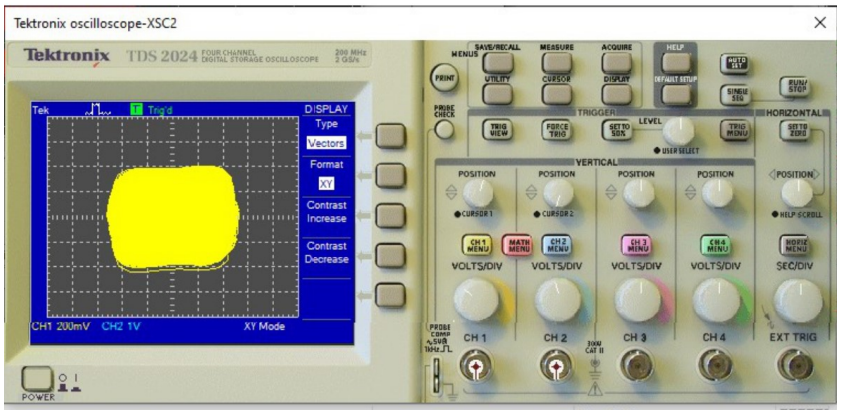

Figure 23: (x, w) plot of the new hyperchaotic system (27) via Tektronix oscilloscope

7. Complete synchronization of the new hyperchaotic systems

To achieve complete synchronization of the new hyperchaotic system taken as the transmitter and receiver systems, we shall employ the integral sliding mode control (ISMC), which is a well-known technique in the control literature and it has several applications in engineering [35].

The transmitter system is taken as the new hyperchaotic system with a curve equilibrium which is given by the 4-D dynamics

$$\begin{cases} \dot{x}_1 = a(y_1 - x_1), \\ \dot{y}_1 = cy_1 - px_1 - x_1z_1 + w_1\,, \\ \dot{z}_1 = x_1y_1 - bz_1\,, \\ \dot{w}_1 = (c-p)x_1 - \dfrac{1}{b}x_1^3 + w_1\,. \end{cases} \tag{32}$$

We denote the state of the transmitter system (32) as $X_1 = (x_1, y_1, z_1, w_1)$.

The receiver system is taken as the new hyperchaotic system with a curve equilibrium and equipped with integral sliding mode controls (ISMC), which is given by the 4-D dynamics

$$\begin{cases} \dot{x}_2 = a(y_2 - x_2) + U_x\,, \\ \dot{y}_2 = cy_2 - px_2 - x_2z_2 + w_2 + U_y\,, \\ \dot{z}_2 = x_2y_2 - bz_2 + U_z\,, \\ \dot{w}_2 = (c-p)x_2 - \dfrac{1}{b}x_2^3 + w_2 + U_w\,. \end{cases} \tag{33}$$

We denote the state of the receiver system (33) as $X_2 = (x_2, y_2, z_2, w_2)$.

Also, we denote $U = (U_x, U_y, U_z, U_w)$ as the integral sliding mode controller (ISMC) to be designed to achieve complete synchronization between (32) and (33).

We define the synchronization error as follows:

$$\begin{cases} E_x = x_2 - x_1\,, \\ E_y = y_2 - y_1\,, \\ E_z = z_2 - z_1\,, \\ E_w = w_2 - w_1\,. \end{cases} \tag{34}$$

We obtain the error dynamics as given below:

$$\begin{cases} \dot{E}_x = a(E_y - E_x) + U_x\,, \\ \dot{E}_y = -pE_x + cE_y + E_w - x_2z_2 + x_1z_1 + U_y\,, \\ \dot{E}_z = -bE_z + x_2y_2 - x_1y_1 + U_z\,, \\ \dot{E}_w = (c-p)E_x + E_w - \dfrac{1}{b}\left(x_2^3 - x_1^3\right) + U_w\,. \end{cases} \tag{35}$$

In the IMSC design, an integral sliding surface is assigned with every synchronization error variable as follows:

$$\begin{cases} S_x = E_x + \mu_x \displaystyle\int_0^t E_x(\tau)\,\mathrm{d}\tau, \\ S_y = E_y + \mu_y \displaystyle\int_0^t E_y(\tau)\,\mathrm{d}\tau, \\ S_z = E_z + \mu_z \displaystyle\int_0^t E_z(\tau)\,\mathrm{d}\tau, \\ S_w = E_w + \mu_w \displaystyle\int_0^t E_w(\tau)\,\mathrm{d}\tau. \end{cases} \tag{36}$$

A simple calculation results in the following dynamics:

$$\begin{cases} \dot{S}_x = \dot{E}_x + \mu_x E_x \,, \\ \dot{S}_y = \dot{E}_y + \mu_y E_y \,, \\ \dot{S}_z = \dot{E}_z + \mu_z E_z \,, \\ \dot{S}_w = \dot{E}_w + \mu_w E_w \,. \end{cases} \tag{37}$$

We consider the integral sliding mode controls defined as follows:

$$\begin{cases} U_x = -a(E_y - E_x) - \mu_x E_x - \alpha_x \operatorname{sgn}(S_x) - k_x S_x \\ U_y = pE_x - cE_y - E_w + x_2 z_2 - x_1 z_1 - \mu_y E_y \\ \qquad - \alpha_y \operatorname{sgn}(S_y) - k_y S_y \\ U_z = bE_z - x_2 y_2 + x_1 y_1 - \mu_z E_z - \alpha_z \operatorname{sgn}(S_z) - k_z S_z \cdot \\ U_w = -(c-p)E_x - E_w + \dfrac{1}{b}\left(x_2^3 - x_1^3\right) - \mu_w E_w \\ \qquad - \alpha_w \operatorname{sgn}(S_w) - k_w S_w \,. \end{cases} \tag{38}$$

In Eq. (38), α_i, μ_i, k_i, $(i = 1, 2, 3, 4)$ are taken as positive constants.
From (35) and (38), we simplify the closed-loop error dynamics as follows:

$$\begin{cases} \dot{E}_x = -\mu_x E_x - \alpha_x \operatorname{sgn}(S_x) - k_x S_x \,, \\ \dot{E}_y = -\mu_y E_y - \alpha_y \operatorname{sgn}(S_y) - k_y S_y \,, \\ \dot{E}_z = -\mu_z E_z - \alpha_z \operatorname{sgn}(S_z) - k_z S_z \,, \\ \dot{E}_w = -\mu_w E_w - \alpha_w \operatorname{sgn}(S_w) - k_w S_w \,. \end{cases} \tag{39}$$

The main ISMC result for the synchronization of master-slave hyperchaotic systems (32) and (33) can be stated as follows.

Theorem 1. *The integral sliding mode control (ISMC) law defined by Eq. (38) achieves global hyperchaos synchronization between the transmitter system (32) and the receiver system (33) for all values of the initial states* $X_1(0), X_2(0) \in \mathbb{R}^4$, *where* α_i, μ_i, k_i, $(i = 1, 2, 3, 4)$ *are taken as positive constants.*

Proof. We use Lyapunov stability theory to prove this result.
We take the Lyapunov function defined by

$$V(S_x, S_y, S_z, S_w) = \frac{1}{2}\left(S_x^2 + S_y^2 + S_z^2 + S_w^2\right). \tag{40}$$

It is clear that V takes only non-negative values. Furthermore, $V = 0$ if and only if $S_x = S_y = S_z = S_w = 0$.

Hence, V is a quadratic and strictly positive definite function on $\mathbb{R}^4$.

A direct calculation shows that

$$\dot{V} = S_x(-\alpha_x \operatorname{sgn}(S_x) - k_x S_x) + S_y(-\alpha_y \operatorname{sgn}(S_y) - k_y S_y) + S_z(-\alpha_z \operatorname{sgn}(S_z) - k_z S_z) + S_w(-\alpha_w \operatorname{sgn}(S_w) - k_w S_w). \quad (41)$$

Simplifying (41), we get

$$\dot{V} = -\alpha_x |S_x| - k_x S_x^2 - \alpha_y |S_y| - k_y S_y^2 - \alpha_z |S_z| - k_z S_z^2 - \alpha_w |S_w| - k_w S_w^2. \quad (42)$$

Thus, $\dot{V}$ is a strictly negative definite function defined on $\mathbb{R}^4$.

Using Lyapunov stability theory, we deduce that $S_x(t) \to 0$, $S_y(t) \to 0$, $S_z(t) \to 0$ and $S_w(t) \to 0$ as $t \to \infty$.

Hence, it follows that $E_x(t) \to 0$, $E_y(t) \to 0$, $E_z(t) \to 0$ and $E_w(t) \to 0$ as $t \to \infty$.

This completes the proof. □

For MATLAB simulations, we take the parameter values as in the hyperchaotic case, *viz.*

$$a = 74, \quad b = 18, \quad c = 40, \quad p = 3. \quad (43)$$

We take the values of ISMC parameters as follows:

$$\alpha_x = 0.4, \quad \alpha_y = 0.4, \quad \alpha_z = 0.4, \quad \alpha_w = 0.4, \quad \mu_x = 5, \quad \mu_y = 5, \quad (44)$$

$$\mu_z = 5, \quad \mu_w = 5, \quad k_x = 10, \quad k_y = 10, \quad k_z = 10, \quad k_w = 10. \quad (45)$$

The initial state of the transmitter system (32) is taken as follows:

$$x_1(0) = 0.5, \quad y_1(0) = 5.9, \quad z_1(0) = 3.8, \quad w_1(0) = 6.4. \quad (46)$$

The initial state of the receiver system (33) is taken as follows:

$$x_2(0) = 4.1, \quad y_2(0) = 2.7, \quad z_2(0) = 5.9, \quad w_2(0) = 0.5. \quad (47)$$

Figure 24 shows the time-plot of the synchronization error between the transmitter system (32) and the receiver system (33).

8. Conclusions

The main contribution of this research work is the mathematical modeling of a new hyperchaotic Lü chaotic system with a curve equilibrium. We obtained this new hyperchaotic system by first modeling a new 3-D chaotic Lü system by modifying the dynamics of the classical Lü chaotic system (2002) and then by introducing a state feedback to the new 3-D modified Lü chaotic system to obtain a new 4-D hyperchaotic Lü system with a curve equilibrium. We presented a

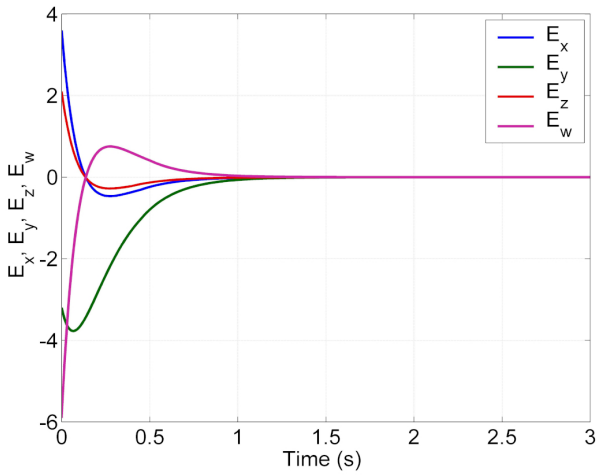

Figure 24: Time-plot of the synchronization error between the transmitter system (32.) and the receiver system (33)

detailed bifurcation analysis of the new 4-D hyperchaotic Lü system with a curve equilibrium and described the bifurcation transition diagrams and Lyapunov exponents diagrams. We also derived new multistability results of the new 4-D hyperchaotic Lü system with a curve equilibrium. For engineering applications, we provided an electronic circuit simulation of the proposed hyperchaotic Lü system using MultiSim 14.0. As a control application, we present new results for complete synchronization for a pair of new hyperchaotic Lü systems taken as the master and slave systems. We use integral sliding mode control (ISMC) to achieve complete synchronization for transmitter and receiver hyperchaotic Lü systems. MATLAB simulations illustrate all the main results of this research work.

References

[1] S. Vaidyanathan and A.T. Azar: *Backstepping Control of Nonlinear Dynamical Systems,* Academic Press, New York, (2020).

[2] Z. Jiang and X. Liu: Image encryption algorithm based on discrete quantum baker map and Chen hyperchaotic system. *International Journal of Theoretical Physics,* **62**(2), (2023). DOI: 10.1007/s10773-023-05277-0

[3] A.D. Mengue, D.E. Essebe and B.Z. Essimbi: High-dimensional hyperchaos and its control in a modified laser system subjected to optical injection. *Optical and Quantum Electronics,* **56**(7), (2024). DOI: 10.1007/s11082-024-06534-0

[4] C. Zhang, H. Wang, Y. Zhang, L. Zhang and C. Ma: Dynamics analysis and DSP implementation of a new four-dimensional discrete memristor hyperchaotic map. *Integration,* **103**, (2025). DOI: 10.1016/j.vlsi.2025.102384

[5] A. Hassan and L. Zhou: A novel 6D four-wing memristive hyperchaotic system: Generalized fixed-time synchronization and its application in secure image encryption. *Chaos, Solitons and Fractals,* **192**, (2025). DOI: 10.1016/j.chaos.2024.115986

[6] Z. Liu, C. Li, C. Zhang and X. Yang: Dual-domain image encryption scheme based on fractional wavelet transform and hyperchaotic system. *Physica Scripta,* **100**(3), (2025). DOI: 10.1088/1402-4896/adb529

[7] Z. Han, Y. Cao, S. Banerjee and J. Mou: Hybrid image encryption scheme based on hyperchaotic map with spherical attractors. *Chinese Physics B,* **34**(3), (2025). DOI: 10.1088/1674-1056/ada7db

[8] N.R. Babu, P. Balasubramaniam and E.M. Joo: Video encryption via synchronization of a fractional order T-S fuzzy memristive hyperchaotic system. *Multimedia Tools and Applications,* **83**(9), (2024), 26055–26088. DOI: 10.1007/s11042-023-16483-7

[9] S. Rajendran and P. Kaliyaperumal: Prescribed-time synchronization of hyperchaotic fuzzy stochastic PMSM model with an application to secure communications. *Applied Mathematics and Computation,* **493**, (2025). DOI: 10.1016/j.amc.2024.129257

[10] S. Hussain, Z. Bashir and M.G.A. Malik: Chaos analysis of nonlinear variable order fractional hyperchaotic Chen system utilizing radial basis function neural network. *Cognitive Neurodynamics,* **18**(5), (2024), 2831–2855. DOI: 10.1007/s11571-024-10118-9

[11] M. Bodke and S. Chaudari: Enhanced selective hyper chaotic encryption using deep neural network for hyperspectral images. *Earth Science Informatics,* **18**(1), (2025). DOI: 10.1007/s12145-024-01684-x

[12] Y. Luo, Q. Liu, X. Che and Z. He: LMF algorithm based on hyper-chaos for the solving of forward displacement in a parallel robot mechanism. *International Journal of Advanced Robotic Systems,* **10**, (2013). DOI: 10.5772/54817

[13] V.-T. Pham, S. Vaidyanathan, C. Volos and T. Kapitaniak: *Nonlinear Dynamical Systems with Self-Excited and Hidden Attractors,* Springer, Berlin, Germany, 2018. DOI: 10.1007/978-3-319-71243-7

[14] Y. Chen and Q. Yang: A new Lorenz-type hyperchaotic system with a curve of equilibria. *Mathematics and Computers in Simulation,* **112**, (2015), 40–44. DOI: 10.1016/j.matcom.2014.11.006

[15] S. Vaidyanathan, I.M. Moroz, E. Tlelo-Cuautle, A. Sambas, C.F. Bermudez-Marquez and S.A. Safaan: Mathematical modeling, bifurcation analysis, circuit design and FPGA implementation of a 5D hyperchaotic weather fluctuation model with a line of equilibrium points. *International Journal of Modelling, Identification and Control,* **43**(4), (2023), 267–283. DOI: 10.1504/IJMIC.2023.10059035

[16] M. Mechekef, L. Meddour and T. Houmor: Generation of a multiwing hyperchaotic system with a line equilibrium and its control. *Journal of Comptuational and Nonlinear Dynamics,* **20**(4), (2025). DOI: 10.1115/1.4067860

[17] N.A. Saeed, H.A. Saleh, L. Hou and E.A. Nasr: A novel chaotic oscillator with a half-line of unstable equilibria: Basins of attraction, chaos control, chaos synchronization, and encryption applications. *Modern Physics Letters B,* **39**(8), (2025). DOI: 10.1142/S0217984924504360

[18] V.T. Pham, S. Jafari, C. Volos and T. Kapitaniak: A gallery of chaotic systems with an infinite number of equilibrium points. *Chaos, Solitons and Fractals,* **93**, (2016), 58–63. DOI: 10.1016/j.chaos.2016.10.002

[19] M.A. Mohamed, T. Bonny, A. Sambas, S. Vaidyanathan, W. Al Nassan, S. Zhang, K. Obaideen, M. Mamat and M.K.M. Nawawi: A speech cryptosystem using the new chaotic system with a capsule-shaped equilibrium curve. *Computers, Materials and Continua,* **75**(3), (2023), 5987–6006. DOI: 10.32604/cmc.2023.035668

[20] J. Ramadoss, R. Kengne, D. Takoue Ngatcha, V. Kamdoum Tamba, K. Rajagopal and M. Motchongom Tingue: A three-dimensional autonomous system with a parabolic equilibrium: Dynamical analysis, adaptive synchronization via relay coupling, and applications to steganography and chaos encryption. *Complexity,* **2022**, (2022). DOI: 10.1155/2022/8362836

[21] J. Lü and G. Chen: A new chaotic attractor coined. *International Journal of Bifurcation and Chaos,* **12**(3), (2002), 659–661. DOI: 10.1142/S0218127402004620

[22] Y. Guang, Q. Ding and Y. Zhang: A novel approach to constructing a parameter-controlled multi-scroll conservative hyperchaotic system: applications in image encryption. *Physica Scripta,* **100**(3), (2025), Article ID 035231. DOI: 10.1088/1402-4896/adb45b

[23] T. Ma, J. Mou and W. Chen: Dynamics and implementation of a functional neuron model with hyperchaotic behavior under electromagnetic radiation. *Chaos, Solitons and Fractals,* **190**, (2025). DOI: 10.1016/j.chaos.2024.115795

[24] M. Kopp and I. Samuilik: A new 6D two-wing hyperchaotic system: Dynamical analysis, circuit design, and synchronization. *Chaos Theory and Applications,* **6**(4), (2024), 273–283. DOI: 10.51537/chaos.1513080

[25] Y. Li and M. Li: Analysis and implementation of a novel parametrically controllable spherical multi-scroll memristive conservative hyperchaotic system. *Integration,* **103** (2025). DOI: 10.1016/j.vlsi.2025.102409

[26] S. Vaidyanathan, A. Sambas, M. Mamat and M. Sanjaya Ws: A new three-dimensional chaotic system with a hidden attractor, circuit design and application in wireless mobile robot. *Archives of Control Sciences,* **27**(4), (2017), 541–554. DOI: 10.1515/acsc-2017-0032

[27] Y. Shen, Z. Chen, Y. Li and W. Li: Coexisting attractors, amplitude control, circuit implementation of grid-scroll memristive hyperchaotic oscillator and its application in underwater signal detection. *Mechanical Systems and Signal Processing,* **229** (2025). DOI: 10.1016/j.ymssp.2025.112525

[28] J. Fang, J. Wang, K. Zhao, Y. Jiang and W. Liang: A new dual memristor hyperchaotic system: dynamic properties, electronic circuit, and image encryption. *Analog Integrated Circuits and Signal Processing,* **122**(2), (2025). DOI: 10.1007/s10470-025-02322-2

[29] J. Yang, Y. Yu, D. Zeng, Y. Hu, J. Liu, K. Liu, G. Carbone, S. Luo and X. Zhu: An adaptive sliding mode fault-tolerant control of variable speed reaching law for steer-by-wire systems. *Scientific Reports,* **15**(1), (2025). DOI: 10.1038/s41598-025-96663-7

[30] V.C. Nguyen and S.H. Kim: A novel fixed-time prescribed performance sliding mode control for uncertain wheeled mobile robots. *Scientific Reports,* **15**(1), (2025). DOI: 10.1038/s41598-025-89126-6

[31] C. Liang, Y. Ding, F. Weng, W. Chen and J. Li: Dual observers based sliding mode control for QUAVs with unknown disturbances and time varying delays. *Scientific Reports,* **15**(1), (2025). DOI: 10.1038/s41598-025-88511-5

[32] S.L. Yan: Study of dual-hyperchaos synchronization between an erbium-doped fiber three-ring laser and an erbium-doped fiber dual-ring laser, and their applications to dual-channel encoding. *Electronics Letters,* **59**(14), (2023). DOI: 10.1049/ell2.12872

[33] Q. Shi, Y. Zhao and Q. Ding: Design and FPGA implementation of encrypted frame transmission scheme based on chaotic reverse synchronization. *Nonlinear Dynamics,* **113**(6), (2025), 5511–5535. DOI: 10.1007/s11071-024-10538-6

[34] J. Llibre, M. Messias and P.R. Da Silva: Global dynamics in the Poincaré ball of the Chen system having invariant algebraic surfaces. *International Journal of Bifurcation and Chaos,* **22**, (2012). DOI: 10.1142/S0218127412501544

[35] S. Vaidyanathan and C.H. Lien: *Applications of Sliding Mode Control in Science and engineering*. Springer, Berlin, Germany, 2017. DOI: 10.1007/978-3-319-55598-0